Available online at www.synsint.com

Synthesis and Sintering

ISSN 2564-0186 (Print), **ISSN** 2564-0194 (Online)

Research article

Effect of chemical composition on fabrication of HAp-YSZ-Ti composites by spark plasma sintering method

Seyyed Mohsen Fatemi, Iman Mobasherpour *, Leyla Nikzad, Mansour Razavi, Leyla Karamzadeh

Ceramics Department, Materials and Energy Research Center (MERC), Karaj, Iran

A B S T R A C T

This research examines the thermal behavior and sintering characteristics of hydroxyapatite (HAp) composites with yttria-stabilized zirconia (YSZ) and titanium via the spark plasma sintering (SPS) method. This study uses simultaneous thermal analysis (STA) to investigate the decomposition behavior of composites. During the sintering process, data on displacement, temperature, time, and current were recorded. A key challenge encountered was the fracture and crushing of the samples after the sintering process. The results show that the decomposition temperature of pure HAp (sample 100-0-0) occurs around 800 °C. In contrast, adding 4% titanium and 6% YSZ to the sample composition increases the decomposition temperature above 1000 °C. A further increase in YSZ content, up to 31%, leads to a decomposition temperature of approximately 1000 °C. These findings show that the presence of titanium and its conversion to TiO_2, together with YSZ, increases the stability of the composite materials and thus reduces HAp decomposition and affects the thermal behavior of the sintered samples.

KEYWORDS

Hydroxyapatite
Yttria-stabilized zirconia
Titanium
Spark plasma sintering
Simultaneous thermal analysis

OPEN ACCESS

1. Introduction

Over time, due to accidents, injuries, and natural problems that happen to humans with age, the need for a suitable artificial bone that can be used as a substitute for human bone is felt. In recent years, much research work has been conducted in this field. Human bone is a composite of hydroxyapatite [$Ca_{10}((PO)_4)_6(OH)_2$], collagen type 1, water, cells, and fats. This shows that chemically, hydroxyapatite (HA) is very similar to bone and can be used as a good candidate for bone. In this material, the calcium-to-phosphorus ratio is 1.67 [1–5].

Most calcium phosphate bioceramics include hydroxyapatite, β-tricalcium phosphate, α-tricalcium phosphate, or combinations of these phases [6–9]. Calcium phosphate can be produced using various processes, including cold isostatic pressing, uniaxial pressing, slurry casting, hot isostatic pressing, jelly casting, injection molding, and extrusion [10–13].

The primary drawback of calcium phosphate-based materials is their brittleness and low fatigue resistance. To enhance the mechanical features of hydroxyapatite, ceramics, and metals can be incorporated as reinforcements [14–16]. The properties of calcium phosphates are influenced by factors like chemical composition (purity and stoichiometry), uniformity, phase distribution, grain size and shape, crystallinity, and the size and distribution of pores [13, 17, 18].

Reinforcing HAp with metals or ceramics has been investigated to improve its biomechanical characteristics. Zr, yttria-stabilized zirconia (YSZ), and Ti are commonly introduced into hydroxyapatite (HA) to improve its mechanical performance and bioactivity. [6, 13, 19].

* Corresponding author. *E-mail address:* i.mobasherpour@merc.ac.ir (I. Mobasherpour)
Received 17 December 2023; Received in revised form 14 August 2024; Accepted 14 August 2024.

https://doi.org/10.53063/synsint.2024.43193

Table 1. The particle size of the used powders.

HA	YSZ	Ti
D10 ≤ 1.355 μm	D10 ≤ 6.020 μm	D10 ≤ 29.791 μm
D50 ≤ 3.878 μm	D50 ≤ 36.771 μm	D50 ≤ 53.816 μm
D90 ≤ 10.520 μm	D90 ≤ 59.391 μm	D90 ≤ 89.169 μm

The spark plasma sintering (SPS) is one of the advanced synthesis methods that has received significant attention in recent decades owing to the use of mechanical pressure and lower sintering time. Recently, the SPS technique has become a widely utilized tool in development of the advanced materials such as ceramics, metals, composites, and polymers [20–24]. The spark plasma sintering method operates under high temperatures (up to 2500 °C) and medium pressure (up to 150 MPa), enabling efficient densification of materials. It facilitates the production of nearly fully dense materials by consolidating powders more quickly and at lower temperatures compared to conventional methods. This technique is characterized by the application of a low-voltage, high-intensity pulsed current that flows through the graphite die containing the powder and then through the sample itself [25–27]. The Joule effect produces rapid heating, reaching up to 1000 °C/min. This high rate of heating, coupled with fast cooling and the application of an external mechanical load, allows the powder to consolidate rapidly at temperatures that are 200 to 500 °C lower than those required for traditional sintering methods. Indeed, the creation of dense nanostructured materials is possible by optimizing kinetic parameters and applying uniaxial pressure to minimize grain coarsening and enhance densification utilizing SPS as a rapid sintering technique. The performance of the SPS technique is largely attributed to the application of a pulsed electric field to the sample throughout the sintering process [28–30].

In this research, the sintering behavior of the HAp-YSZ-Ti composite was investigated via the plasma spark sintering technique. The effect of the chemical composition of the composite on the amount of displacement during the plasma spark sintering process and changes in the vacuum pressure of the process were studied.

2. Experimental Procedure

2.1. Materials

In this work, hydroxyapatite (HAp), titanium (Ti), and zirconia powders stabilized with yttria (YSZ) were used. The HAp powder, in micron size, was purchased from the German Merck brand (E. Merck, D-6100 Darmstadt F.R. Germany). Also, commercial powders of yttria-stabilized zirconia (ZrO_2-3 mol% Y_2O_3 from Hebei Suoyi New Material Technology Co., Ltd.) and titanium (Baoji Yumingda Metal Materials Co., Ltd.) both in micron sizes were used. The particle sizes of the raw material powders are presented in Table 1.

2.2. Preparation

Composite samples were manufactured using different powders with varying weight percentages and maximum sintering temperatures. These values, along with the sample codes, are listed in Table 2.

To fabricate the samples, first, the powders were weighed according to the weight composition specified in Table 2, with an accuracy of 0.0001 g, and then they were mixed in a ball mill for 1 h to mix evenly.

2.3. Spark plasma sintering

In this study, the samples were produced using the spark plasma sintering technique. The inner diameter of the used mold was 30 mm. After covering the inner wall of the mold with thin flexible graphite foil, 10 g of the prepared powder was added to the mold and compacted using a mandrel. The mold was placed in the machine. A thermocouple was used to measure the temperature. After the vacuum value reached below 50 Pa, the heating of the sample was started by gradually increasing the current. The initial pressure was selected at 10 MPa, and the current increased at a rate of about 0.08 A/min, resulting in the heating of the sample. During the sintering process, the pressure increased to 30 MPa. The samples were held at the maximum sintering temperature for 5 min before cooling, which was achieved by gradually reducing the current. During the sintering process, temperature, displacement, time, and current were recorded. Using these data, various graphs were drawn, such as displacement versus time, temperature versus time, etc.

2.4. Characterizations

Simultaneous thermal analysis (STA) test was used to check the thermal behavior of the samples. For this purpose, 1 g of each powder sample with the compositions coded 100-0-0, 90-6-4, and 65-31-4 was used. The experiments were conducted in an argon atmosphere, with the samples evaluated over a temperature range of 20–1000 °C at a heating rate of 10 °C/min. For this purpose, 1 g of three powder samples with the same composition of codes 100-0-0, 90-6-4, and 65-31-4 were used. The atmosphere of this experiment was argon gas, and the samples were evaluated in the temperature range of 20–1000 °C with a speed of 10 °C/min. An X-ray diffraction test was employed to determine the type of phases formed. Cu (Kα) beam was used as an X-ray source. The residence time for each step was 1 s, with a step size of 0.02 °, and the scanning range was set between 20 ° and 70 °. To determine the phases in the samples, the obtained X-ray diffraction patterns were matched with JCPDS standards using X'Pert software. The microstructure of the samples was examined using an ultra-high vacuum, high-resolution field emission scanning electron microscope (FESEM: Mira3 Tescan) operated at 20 kV. The samples were prepared by gold sputtering at a low deposition rate.

Table 2. Chemical composition and sintering temperature of prepared samples.

Sample code	Composition (wt%)	Sintering temperature (°C)
100-0-0	100% HA	750
90-6-4	90% HA-6% YSZ-4% Ti	800
65-31-4	65% HA-31% YSZ-4% Ti	880

3. Results and discussion

3.1. Investigation of simultaneous thermal analysis

A simultaneous thermal analysis (STA) test was utilized to examine the thermal behavior of the specimens. The results of the STA test for samples 100-0-0, 90-6-4, and 65-31-4 are shown in Fig. 1.

As shown in Fig. 1, the weight of sample 100-0-0 decreased to 92.5% of its initial weight by approximately 560 °C, indicating a weight loss of about 7.5% up to this temperature. From approximately 560 to 800 °C, the slope of the ΔT graph changed. By the temperature of 800 °C, the weight of the sample had decreased to 84% of its initial weight. At this temperature, an endothermic reaction occurred. It was found that as the temperature The outflow of network water results in the oxyhydroxyapatite (OHA) formation that creates vacancies in the hydroxyl group spaces within the hydroxyapatite structure [31].

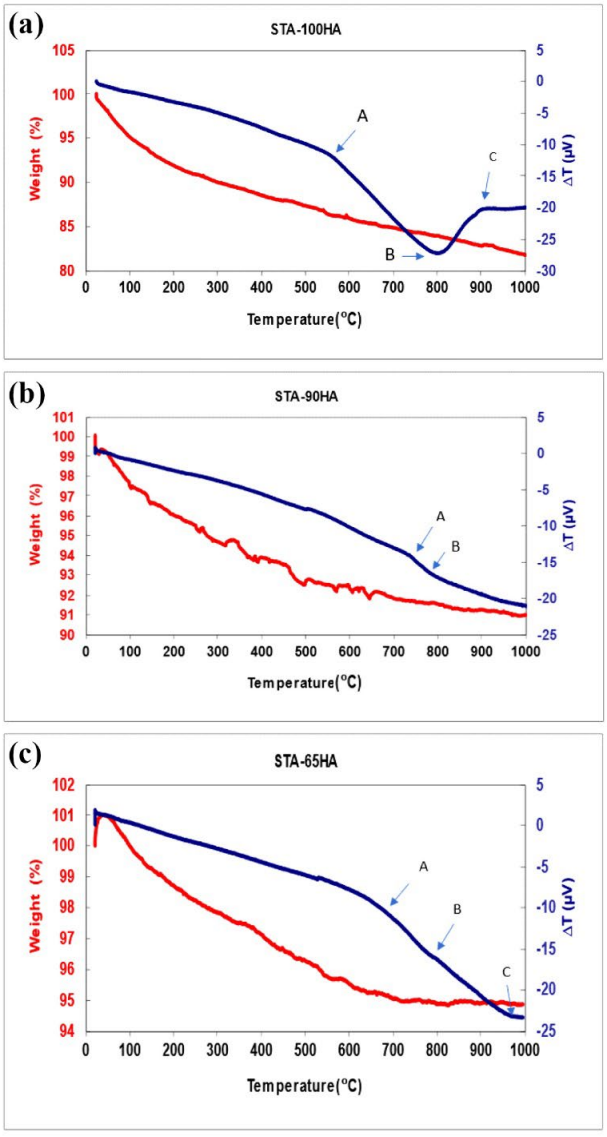

Fig. 1. Simultaneous thermal analysis (STA) curve of samples: a) 100-0-0, b) 90-6-4, and c) 65-31-4.

From point A in Fig. 1a (560 °C), the thermal decomposition of hydroxyapatite starts and continues up to 900 °C (point C in 100-0-0 sample). The highest amount of decomposition occurs at 800 °C (point B in 100-0-0 sample). The reaction at this temperature is related to the thermal decomposition of hydroxyapatite and the tricalcium phosphate (TCP) formation.

The curve of the 90-6-4 sample displays a change in the slope of the ΔT diagram at 730 °C (point A in Fig. 1b). Up to this temperature, the weight of the sample reached 91.8% of the initial weight, showing a 2.8% weight loss. From this temperature onwards, the weight of the sample remained nearly constant up to 1000 °C. The weight of the 65-31-4 sample decreased until it reached 700 °C, leading to a 5% weight loss, or 95% of the initial weight remaining.

In the examined composites, the decomposition of hydroxyapatite in the presence of zirconia, despite its inherent stability as a single phase up to 1300 °C, can be attributed to the reduced stability caused by the interaction with the secondary component. In the yttria-stabilized zirconia composite, the calcium oxide produced from the decomposition dissolves into the structure of the zirconia, resulting in the following relationship [32]:

$$CaO + Y\text{–doped } ZrO_2(t) \rightarrow Ca,Y\text{–Doped } ZrO_2(t) \quad (1)$$

Therefore, the general decomposition relationship will be as follows [32]:

$$Ca_{10}(PO_4)_6(OH)_2 + Y\text{–}ZrO_2(t) \rightarrow 3\beta\text{–}Ca_3(PO_4)_2 + CaO\text{–doped } Y\text{–}ZrO_2(c)/Y\text{–doped } CaZrO_3 + H_2O \quad (2)$$

The presence of partially stabilized tetragonal zirconia reduces the extent of hydroxyapatite decomposition. Partially yttria-stabilized zirconia has a lower reactivity with calcium oxide. Yttria reduces the penetration coefficient of calcium oxide in zirconia by closing the structural defects of zirconia. This blockage of penetration paths creates fewer paths for calcium oxide to penetrate the zirconia structure. The formation temperature of $CaZrO_3$ in the composite containing pure zirconia is 1300 °C. However, in yttria-stabilized zirconia, this temperature decreases due to the restricted penetration of calcium oxide into the zirconia lattice, leading to supersaturation on the zirconia surface.

In the ΔT curve of the sample 90-6-4, point A marks the onset of the endothermic reaction of hydroxyapatite decomposition, beginning at the temperature of 730 °C. Additionally, the ΔT curve trends toward its lowest value, which will occur at a temperature above 1000 °C, correspond to the peak of the hydroxyapatite decomposition reaction.

In the 65-31-4 curve, point A shows the onset of the endothermic reaction of hydroxyapatite decomposition, which begins at 700 °C, and the curve peak is around 1000 °C (point C). As it is clear from the results, the weight loss up to 560 °C is due to the release of network and absorbed water, and this weight loss decreases as the amount of hydroxyapatite in the sample composition is reduced. Additionally, the decomposition reaction of pure hydroxyapatite typically occurs around 800 °C. However, the decomposition temperature of hydroxyapatite increases to above 1000 °C as 4% titanium and 6% YSZ are added to the sample composition. With further YSZ addition, up to 31% in the composition of the sample, the decomposition temperature stabilizes at approximately 1000 °C.

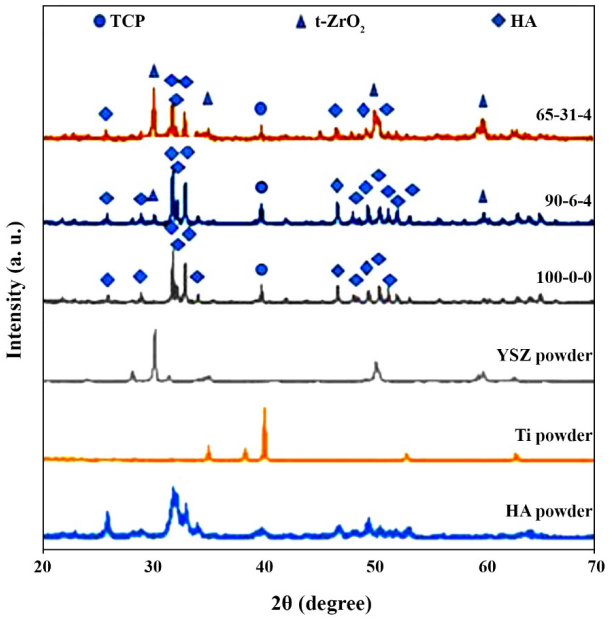

Fig. 2. X-ray diffraction analysis of samples.

This phenomenon is probably attributed to the low amount of YSZ in the sample 90-6-4. Since the YSZ structure requires less CaO content to reach saturation after the titanium addition, the decomposition of hydroxyapatite is reduced.

In sample 65-31-4, the further content of YSZ requires a greater amount of stabilizing material, leading to more hydroxyapatite decomposition. Therefore, the decomposition temperature of hydroxyapatite in sample 65-31-4 is lower compared to that in sample 90-6-4.

Based on the examination of the simultaneous thermal analysis curve and other analyses, a maximum plasma spark sintering temperature of 750 °C was considered for the sample 100-0-0. For the samples 90-6-4 and 65-31-4, the maximum processing temperatures were selected at 800 °C and 880 °C, respectively.

3.2. Crystalline phase analysis

The phase composition of the as-sintered specimens was determined by XRD analysis, and the results were subsequently analyzed using X'Pert HighScore software. Fig. 2 presents the XRD test results for samples 100-0-0, 90-6-4, and 65-31-4, along with the diffraction patterns of the pure powders of Ti, HA, and YSZ.

The pure HA has a short and broad peak which indicates its lower crystallinity and more amorphous nature. The samples 100-0-0, 90-6-4, and 65-31-4 exhibit sharp peaks with narrow widths, indicating their high crystallinity. The detection of the TCP phase in the results indicates that some decomposition of HA occurred during the sintering process.

The TCP phase increased in the sample 90-6-4 compared to the sample 100-0-0 but decreased again in the sample 65-31-4. This change may be attributed to the presence of Ti. The thermal decomposition of hydroxyapatite results in the formation of the tricalcium phosphate phase based on the following reaction (Eq. 3) [32].

$$Ca_{10}(PO_4)_6(OH)_2 \rightarrow 3Ca_3(PO_4)_3 + CaO + H_2O \quad (3)$$

Also, the presence of Ti can affect the following reactions [10]:

$$Ti + 2H_2O(g) \rightarrow TiO_2 + 2H_2(g) \quad (4)$$

$$Ca_{10}(PO_4)_6(OH)_2 + TiO_2 \rightarrow Ca_3(PO_4)_2 + CaTiO_3 + H_2(g) + 1/2O_2(g) \quad (5)$$

The presence of Ti, which is converted to TiO_2 together with CaO, can interact with zirconia similarly to yttria. This interaction helps to fully saturate and stabilize the zirconia structure. As a result, the stability of YSZ in the sample 65-31-4 is increased and results in a decrease in the intensity of the TCP phase. Also, as the amount of YSZ increased, the intensity of the tetragonal zirconia peak increased. Additionally, because of the low value of Ti in the as-sintered samples, this phase was not detected.

3.3. FESEM analysis

Fig. 3 displays the FESEM images of the samples. As seen from the images, in sample 90-6-4, sintering and particle bonding are more effective compared to sample 100-0-0. However, there is a higher number of open pores in sample 90-6-4. In sample 65-31-4, a smaller

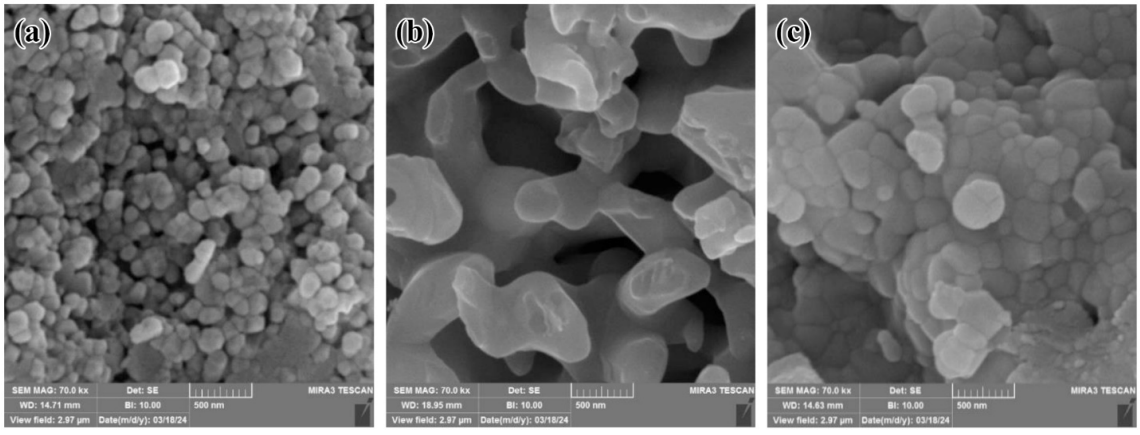

Fig. 3. FESEM analysis of samples: a) 100-0-0, b) 90-6-4, and c) 65-31-4.

number of pores can be seen, which was due to better sintering compared to sample 90-6-4.

3.4. Sintering behavior

According to Table 1, the samples 100-0-0, 90-6-4, and 65-31-4 were sintered. The resulting graphs of displacement and temperature changes over sintering time, and the diagrams of vacuum and temperature variations with respect to sintering time, are presented in Fig. 4.

Based on the STA test results and the gas emission graphs of the sintered samples, two to three distinct gas emissions were observed. The initial gas release occurred in the temperature range of 30–689 °C, corresponding to the release of network and absorbed water. As heating continued, a second gas release was observed. This gas release began and ended simultaneously with the start and end of the sintering process in the samples.

Since SPS is a pressurized sintering method based on electric discharge and spark generation, the electrical discharge at the gaps or junctions between powder particles produces localized heating. This localized heating results in an immediate temperature increase to over 10000 °C in the discharge column [33]. This high temperature causes the evaporation of impurities and also the surface evaporation of powder particles in the spark range. The third gas release, observed at around 850 °C and slightly higher in the sintered sample 65-31-4, was attributed to the decomposition of hydroxyapatite. It was observed that the SPS process, including sparking on the surface of the powders, led to the hydroxyapatite decomposition at the surface and in the parts adjacent to the sparks. A second gas release, which occurred simultaneously with the sintering process, resulted from this decomposition reaction on the powder surfaces.

The displacement measured for samples 100-0-0, 90-6-4, and 65-31-4 was 11.1, 7.9, and 7.4 mm, respectively. It was found that by decreasing the amount of hydroxyapatite and increasing the amount of YSZ, the amount of displacement decreased, which could be due to the lower density of hydroxyapatite.

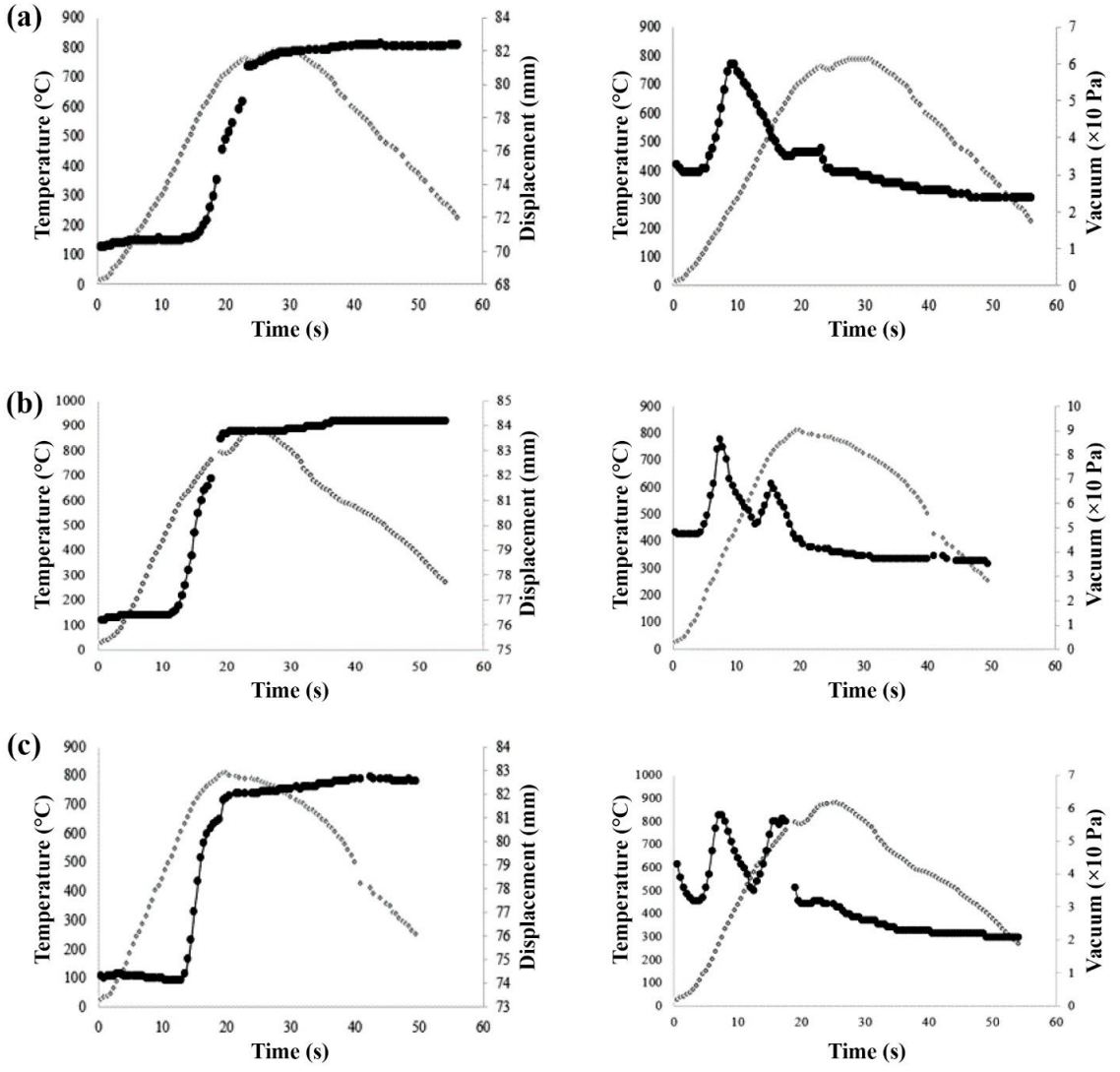

Fig. 4. Displacement and temperature variations versus sintering time as well as vacuum and temperature variations versus sintering time in different samples: a) 100-0-0, b) 90-6-4, and c) 65-31-4.

4. Conclusions

Based on the simultaneous thermal analysis and subsequent analysis, the maximum sintering temperature was set at 750 °C for the sample 100-0-0. For the samples 90-6-4 and 65-31-4, the maximum sintering temperatures were considered 800 °C and 880 °C, respectively. It was found that as the amount of hydroxyapatite decreased and the amount of YSZ increased, the displacement also decreased. The decomposition reaction of pure hydroxyapatite occurs around 800 °C. However, by adding 4% Ti and 6% YSZ to the sample composition, the decomposition temperature of hydroxyapatite increased. By adding more YSZ, up to 31% in the composition of the sample, the decomposition temperature reached above 1000 °C. The presence of titanium, which is converted to TiO_2 together with CaO, can penetrate the structure of zirconia to some extent like yttria. This penetration leads to complete saturation and stability and thus increases the stability of YSZ in the 65-31-4 sample. As a result, this increased stability resulted in less decomposition of hydroxyapatite, which was evident as a decrease in the peak intensity of the TCP phase in sample 65-31-4.

CRediT authorship contribution statement

Seyyed Mohsen Fatemi: Formal analysis, Investigation, Methodology, Writing - original draft.
Iman Mobasherpour: Validation, Writing - review & editing; Project administration.
Leyla Nikzad: Conceptualization, Supervision.
Mansour Razavi: Validation, Supervision.
Leyla Karamzadeh: Investigation, Methodology.

Data availability

The data underlying this article will be shared on reasonable request to the corresponding author.

Declaration of competing interest

The authors have no relevant financial or non-financial interests to disclose.

Funding and acknowledgment

The authors declare that no funds, grants, or other support were received during the preparation of this manuscript.

References

[1] I. Antoniac, M. Negrusoiu, M. Mardare, C. Socoliuc, A. Zazgyva, M. Niculescu, Adverse local tissue reaction after 2 revision hip replacements for ceramic liner fracture, Medicine (Baltimore). 96 (2017) e6687. https://doi.org/10.1097/MD.0000000000006687.

[2] C. Tecu, A. Antoniac, G. Goller, M.G. Gok, M. Manole, A. Mohan, H. Moldovan, K. Earar, The sintering behaviour and mechanical properties of hydroxyapatite - based composites for bone tissue regeneration, Rev. Chim. 69 (2018) 1272–1275. https://doi.org/10.37358/RC.18.5.6306.

[3] B.I. Andrei, M. Niculescu, G. Popescu, Position of anterior cruciate ligament after single-bundle arthroscopic reconstruction, Int. Orthop. 40 (2016) 393–397. https://doi.org/10.1007/s00264-015-2964-7.

[4] O. Mishchenko, A. Yanovska, O. Kosinov, D. Maksymov, R. Moskalenko, et al., Synthetic calcium–phosphate materials for bone grafting, Polymers (Basel). 15 (2023) 3822. https://doi.org/10.3390/polym15183822.

[5] L. Karamzadeh, E. Salahi, I. Mobasherpour, A. Rajabi, M. Javaheri, Characterization of nano-hydroxyapatite synthesized from eggshells for absorption of heavy metals, Synth. Sinter. 3 (2023) 241–247. https://doi.org/10.53063/synsint.2023.34190.

[6] F. Anene, C. Jaafar, A. Mohamed Ariff, I. Zainol, S. Mohd Tahir, et al., Biomechanical properties and corrosion resistance of plasma-sprayed fish scale hydroxyapatite (FsHA) and FsHA-doped yttria-stabilized zirconia coatings on Ti–6Al–4V alloy for biomedical applications, Coatings. 13 (2023) 199. https://doi.org/10.3390/coatings13010199.

[7] T.V. Safronova, I.I. Selezneva, S.A. Tikhonova, A.S. Kiselev, G.A. Davydova, et al., Biocompatibility of biphasic α,β-tricalcium phosphate ceramics in vitro, Bioact. Mater. 5 (2020) 423–427. https://doi.org/10.1016/j.bioactmat.2020.03.007.

[8] C. Xu, Y. Sun, J. Jansen, M. Li, L. Wei, et al., Calcium phosphate ceramics and synergistic bioactive agents for osteogenesis in implant dentistry, Tissue Eng. Part C Methods. 29 (2023) 197–215. https://doi.org/10.1089/ten.tec.2023.0042.

[9] A. Jangjoo Tazeh Kand, F. Afaghi, A. Taghizadeh Tabrizi, H. Aghajani, H. Demir Kivrak, Electrochemical evaluation of the hydroxyapatite coating synthesized on the AZ91 by electrophoretic deposition route, Synth. Sinter. 1 (2021) 85–91. https://doi.org/10.53063/synsint.2021.1226.

[10] A.M. Abraham, S. Venkatesan, A critical review on biomaterials using powder metallurgy method, Eng. Res. Express. 6 (2024) 012508. https://doi.org/10.1088/2631-8695/ad35a6.

[11] K. Jaroszewska, B. Szczęśniak, B. Szyja, J. Choma, M. Jaroniec, Inorganic mesoporous oxides: From research to industrial applications, Mater. Today. 72 (2024) 255–281. https://doi.org/10.1016/j.mattod.2023.11.017.

[12] M.F. Zawrah, M.A. Taha, R.A. Youness, Advanced ceramics: stages of development, Springer Nature, Switzerland. (2024) 1–46. https://doi.org/10.1007/978-3-031-43918-6_1.

[13] M. Prakasam, J. Locs, K. Salma-Ancane, D. Loca, A. Largeteau, L. Berzina-Cimdina, Fabrication, properties and applications of dense hydroxyapatite: a review, J. Funct. Biomater. 6 (2015) 1099–1140. https://doi.org/10.3390/jfb6041099.

[14] M. Furko, K. Balázsi, C. Balázsi, Calcium phosphate loaded biopolymer composites—a comprehensive review on the most recent progress and promising trends, Coatings. 13 (2023) 360. https://doi.org/10.3390/coatings13020360.

[15] D.O. Obada, S.A. Osseni, H. Sina, A.N. Oyedeji, K.A. Salami, et al., Hydroxyapatite materials-synthesis routes, mechanical behavior, theoretical insights, and artificial intelligence models: a review, J. Aust. Ceram. Soc. 59 (2023) 565–596. https://doi.org/10.1007/s41779-023-00854-2.

[16] A. Niakan, S. Ramesh, P. Ganesan, C.Y. Tan, J. Purbolaksono, et al., Sintering behaviour of natural porous hydroxyapatite derived from bovine bone, Ceram. Int. 41 (2015) 3024–3029. https://doi.org/10.1016/j.ceramint.2014.10.138.

[17] L. Vaiani, A. Boccaccio, A.E. Uva, G. Palumbo, A. Piccininni, et al., Ceramic materials for biomedical applications: an overview on properties and fabrication processes, J. Funct. Biomater. 14 (2023) 146. https://doi.org/10.3390/jfb14030146.

[18] Q. Li, C. Feng, Q. Cao, W. Wang, Z. Ma, et al., Strategies of strengthening mechanical properties in the osteoinductive calcium phosphate bioceramics, Regen. Biomater. 10 (2023) rbad013. https://doi.org/10.1093/rb/rbad013.

[19] C.R.D. Ferreira, A.A.G. Santiago, R.C. Vasconcelos, D.F.F. Paiva, F.Q. Pirih, et al., Study of microstructural, mechanical, and biomedical properties of zirconia/hydroxyapatite ceramic composites, Ceram. Int. 48 (2022) 12376–12386. https://doi.org/10.1016/j.ceramint.2022.01.102.

[20] J. Li, M. Fiato, Y. Wu, Transparent high entropy garnet ceramics by SPS, J. Eur. Ceram. Soc. 44 (2024) 7846–7854. https://doi.org/10.1016/j.jeurceramsoc.2024.05.063.
[21] M. Sakkaki, M. Foroutani, P. Zare, Effects of die geometry and insulation on the energy and electrical parameters analyses of spark plasma sintered TiC ceramics, Synth. Sinter. 4 (2024) 4–16. https://doi.org/10.53063/synsint.2024.41172.
[22] S. Otake, H. Sakaguchi, Y. Yoshikawa, T. Kato, D. Nakauchi, et al., Concentration dependence on scintillation properties of BaCl2:Yb transparent ceramics prepared by SPS method, Opt. Mater. (Amst). 154 (2024) 115747. https://doi.org/10.1016/j.optmat.2024.115747.
[23] P. Golmohammadi, A. Bahmani, N. Parvin, B. Nayebi, On the synthesis and sintering behavior of a novel Mg-Ca alloy, Part II: Spark plasma sintering, Synth. Sinter. 4 (2024) 154–159. https://doi.org/10.53063/synsint.2024.42194.
[24] S. Zhang, Z. Teng, L. Wu, C. Chen, Y. Tan, X. Zhou, Rapid preparation of traditional and high-entropy garnet ceramics by SPS at low temperature with ultrafast densification, Ceram. Int. 50 (2024) 4573–4580. https://doi.org/10.1016/j.ceramint.2023.11.197.
[25] Y. Le Godec, S. Le Floch, Recent developments of high-pressure spark plasma sintering: an overview of current applications, challenges and future directions, Materials (Basel). 16 (2023) 997. https://doi.org/10.3390/ma16030997.
[26] X.Y. Li, Z.H. Zhang, X.W. Cheng, G.J. Huo, S.Z. Zhang, Q. Song, The development and application of spark plasma sintering technique in advanced metal structure materials: A review, Powder Metall. Met. Ceram. 60 (2021) 410–438. https://doi.org/10.1007/s11106-021-00254-w.
[27] M. Abedi, S. Sovizi, A. Azarniya, D. Giuntini, M.E. Seraji, et al., An analytical review on Spark Plasma Sintering of metals and alloys: from processing window, phase transformation, and property perspective, Crit. Rev. Solid State Mater. Sci. 48 (2023) 169–214. https://doi.org/10.1080/10408436.2022.2049441.
[28] T.M. Vidyuk, M.A. Korchagin, D.V. Dudina, B.B. Bokhonov, Synthesis of ceramic and composite materials using a combination of self-propagating high-temperature synthesis and spark Plasma sintering (review), Combust. Explos. Shock Waves. 57 (2021) 385–397. https://doi.org/10.1134/S0010508221040018.
[29] X. Li, Z. Guo, Q. Huang, C. Yuan, Research and application of biomimetic modified ceramics and ceramic composites: A review, J. Am. Ceram. Soc. 107 (2024) 663–697. https://doi.org/10.1111/jace.19490.
[30] M. Tokita, Progress of spark plasma sintering (SPS) method, systems, ceramics applications and industrialization, Ceramics. 4 (2021) 160–198. https://doi.org/10.3390/ceramics4020014.
[31] Z. Ebrahimi Kahoo, N. Akrami, M. Ghanad, S. Nazarnezhad, S. Kargozar, S. Mollazadeh, The effect of chemical composition on sintering process and microstructural, mechanical, and biological properties of hydroxyapatite/borate glass composites, J. Met. Mater. Eng. 33 (2022) 111–132. https://doi.org/10.22067/jmme.2022.73523.1032.
[32] S. Salehi, M.H. Fathi, K. Raeissi, Fabrication and characterization of nanostructured hydroxyapatite (HA)/ yttria stabilized zirconia (YSZ) composite coatings with various contents of yttria, J. Adv. Mater. Eng. 29 (2010) 31–43.
[33] Z. Ahmadi, M. Shahedi Asl, M. Zakeri, M. Farvizi, On the reactive spark plasma sinterability of ZrB2–SiC–TiN composite, J. Alloys Compd. 909 (2022) 164611. https://doi.org/10.1016/j.jallcom.2022.164611.